Integrative Biology

Accepted Manuscript

ROYAL SOCIETY OF CHEMISTRY

www.rsc.org/ibiology

Insight box

The paper presents an engineered 3D model of mammary gland that accommodates physiological features of tissue development and remodeling under hormonal control. Porous scaffolds fabricated from collagen and hyaluronan allow for the delivery of multiple cell types in 3D, at staged time points, accommodating the flux of migratory cells present in real tissues. We observed the physiological expression of an important regulator of cell death and oncogenic processes, Stat3, confirming the suitability of our model for studies of cancer biology. We anticipate that organotypic models of this type could contribute future diagnostic and drug discovery platforms for personalized medicine.

A 3-D *in vitro* co-culture model of mammary gland involution

Jonathan J. Campbell[1], Laur-Alexandru Botos[1], Timothy J. Sargeant[1], Natalia Davidenko[2], Ruth E. Cameron[2] and Christine J. Watson[1].

[1.] Department of Pathology and Materials Science and Metallurgy, University of Cambridge,
Tennis Court Road, Cambridge CB2 1QP, UK
[2.] Department of Materials Science and Metallurgy, 27 Charles Babbage Road, Cambridge CB3 0FS

Abstract.

Involution is a process whereby the mammary gland undergoes extensive tissue remodelling involving exquisitely coordinated cell death, extracellular matrix degradation and adipose tissue regeneration following the weaning of offspring. These processes are mediated in part through Jak/Stat signalling pathways, which can be deregulated in breast cancer. Synthetic *in vitro* analogues of the breast could become important tools for studying tumorigenic processes, or as personalized drug discovery platforms and predictors of therapeutic response. Ideally, such models should support 3D neo-tissue formation, so as to recapitulate physiological organ function, and be compatible with high-throughput screening methodologies. We have combined cell lines of epithelial, stromal and immunological origin within porous engineered collagen matrices, demonstrating 3D specific molecular signatures. Furthermore seeded cells form mammary-like branched tissues, with lobuloaveolar structures that undergo inducible involution phenotypes reminiscent of the native gland under hormonal/cytokine regulation. We confirm that autophagy is mediated within differentiated mammary epithelial cells in a Stat-dependent manner at early time points following the removal of a prolactin stimulus (H/WD). In addition, epithelial cells express markers of an M2 macrophage lineage under H/WD, a process that is attenuated with the introduction of the monocyte/macrophage cell line RAW 264.7. Thus, such 3D models are suitable platforms for studying cell-cell interactions and cell death mechanisms in relation to cancer.

Introduction.

The heterogeneity of cancer and the variation in tumour cell sensitivity to therapeutic compounds between individuals is a known difficulty in delivering effective treatments. *In vitro* 3D tissue models are promising candidates for development into high-throughput

screening tools with the potential to be formulated to an individual's requirements through inclusion of biopsy material. We have developed a 3D model of the mammary gland, combining cells of epithelial and stromal origin within defined engineered environments that can be adapted to this task, and can be utilised also for studies of normal mammary gland development [1].

The mammary gland is a dynamic organ that undergoes a highly orchestrated process of cell death and tissue remodelling, known as post-lactational involution following the weaning of offspring. Involution results in progressive loss of milk-producing epithelial tissue and ECM degradation together with re-emergence of the adipose compartment. These processes are governed at a tissue level by numerous factors including LIF and OSM, members of the IL-6 family of cytokines that mediate gene expression primarily through members of the Stat family of transcription factors [2]. Indeed studies of JAK/Stat signalling deregulation in breast cancer have identified Stat3 as an important oncogene that adopts a constitutive mode of action in tumorigenic cells [3]. Furthermore, the microenvironment of the involuting gland is conducive to the development and metastatic progression of breast tumours [4] and has been linked to pregnancy-associated breast cancer [5,6].

Involution is marked by two defined phases, the first of which is reversible and triggered by milk stasis in the gland whilst the second commences with the expression of matrix metalloproteases (MMPs) [7] at approximately 48hrs involution *in vivo*. Interestingly it is not until this later phase in which there is gross destruction and remodelling of glandular tissue that the activation of classical apoptosis mechanisms become apparent. Our laboratory has previously shown that not only is cell death abated and involution delayed with the conditional deletion of Stat3 [8], but that involution precedes in the absence of executioner caspases and is accomplished by Stat3 controlled lysosomal-mediated programmed cell death[9]. Stat3 has been shown to regulate autophagy [10] in liver and *in vitro,* and first phase involution is accompanied by the induction of autophagy as determined by the appearance of LC3 puncta[11]. Moreover, involution is perturbed by ablation of the key regulator of autophagy Atg7. The link between Stat3 signalling and the control of autophagic mechanisms is particularly important considering that *beclin1*-mediated defective autophagy leads to increased tumorigenesis and increased p62, causing mitochondrial damage and the generation of reactive oxygen species[12].

Post-lactational involution is analogous to a wound healing response involving complex epithelial-stromal cell interactions, the activation of elements of both innate and adaptive

immune systems and expression of inflammatory cytokines and proteinases. The interdependence of multiple tissue types is critical for coordinated tissue remodelling, for example the degradation of basement membrane is driven by protease production originating from the fibroblastic component of the tissue[7]. Likewise, tissue resident and infiltrating bone marrow derived macrophages have been implicated in both post-natal mammary developmental and tissue remodelling processes[13,14]. It is well established that a reduction in macrophage number leads to an impairment of ductal morphogenesis during pregnancy[15] while specific depletion in the involuting mammary gland leads to a reduction in both lysosomal-mediated and apoptotic cell death[14]. In addition mammary gland repopulating stem cells have a reduced ability to transplant in colony stimulating factor (CSF) depleted glands[16]. Involution is associated with the polarization of macrophages away from a pro-inflammatory (M1) phenotype to an alternatively activated (M2) state, a phenotypic switch prevalent in a number of regenerating tissues [17,18], and recent work by our laboratory confirms that this polarization is Stat3 dependent and occurs within an infiltrating macrophage population from day 3 of involution[19].

Recognising the potency of, and requirement for, more physiological mammary gland models, the susceptibility of the involuting gland to tumorigenesis and the wide-ranging role of Stat3 in multiple aspects of involution led us to adapt our pre-existing 3D mammary model to studies of involution. Here we report that our model system recapitulates many aspects of this process *in vitro,* displaying Stat3 mediated cell death mechanism and supporting the interaction of epithelial, adipocyte and immune cells consistent with the native gland. We anticipate that such models will become an important resource for studies of tumorigenesis and drug discovery in addition to basic biology.

Results and Discussion

Porous 3D collagen based scaffolds confer physiological relationships to seeded cells.

Involution involves co-ordinated cell death and tissue degradation, so any synthetic model must firstly support 3D physiological tissue formation with associated lumenogenesis and epithelial polarity. We demonstrated previously that porous freeze-dried collagen scaffolds supported growth of the KIM-2 mammary epithelial cell line to form bi-layered polarised ducts and acini [1]. We show here that formation of these structures is associated with expression of specific proteins only in 3D culture. We analysed protein expression in KIM-2 cells grown for 96hrs on tissue culture plastic, 2D collagen films and 3D porous scaffolds (Fig1a). Collagen films and scaffolds were fabricated in the same batch to ensure both 2D and

3D surfaces were biochemically constant. It was noted that the 32kDa form of aquaporin-5 (AQP5), a water transport molecule expressed at the apical domain of various polar epithelial tissues [20], was solely expressed under 3D culture conditions as visualised by immunoblotting (Fig 1a). This is likely to be the glycosylated form of AQP5 [21,22] as opposed to the lower molecular species present in all three culture conditions, and indicates that the 3D culture environment of our system confers functionality to *in vitro* cultured epithelial cells. Glycosylation has been shown to be necessary for appropriate localization of aquaporin protein complexes to the plasma membrane of MDCK cells [23].

Further experiments were conducted using the 3D freeze-dried, cross-linked collagen/hyaluronic acid scaffolds[24] supporting a co-culture of 3T3-L1 differentiated adipocytes together with KIM-2 cells, on the basis of previous data suggesting their support for mammary organoid formation favouring an alveolar-like phenotype[1]. Model setup involved the sequential seeding of 3T3-L1 cells, differentiated with adipogenic supplementation for a total of 2 weeks, prior to the introduction of KIM-2 cells (Fig 1b). Scaffolds were inoculated with both cell types at an initial seeding density of $1x10^6$ cells/mL. KIM-2 cells were allowed to establish in co-culture supplemented in maintenance media (+EGF 10ng/mL) for a further 3 days prior to lactogenic hormone differentiation with PRL, dexamethasone and insulin, for 2 weeks. At this stage KIM-2 cells formed intercommunicating, polar ductal and alveolar-like structures with multiple isolated and intercommunicating lumens that demonstrated apical expression of AQP5 and the tight junction marker ZO-1 (Fig 1c,d). AQP5 is strongly expressed in virgin ducts[25], but only weakly in lactational alveoli[26] and it is interesting to note varying expression levels between organoids in the present study, possibly indicating the presence of both alveolar-type and ductal-type organoids. These organoids were surrounded by basement membrane as demonstrated by the organization of laminin (Fig 1d) and fatty tissue as shown by perilipin staining (Fig 1e).

KIM-2 cells undergo physiological involution-type signalling under 3T3-L1 co-culture conditions.

Our scheme for inducing an *in vitro* involution phenotype exploits the dependency of differentiated KIM-2 cells for prolactin (PRL) mediated survival signalling. Firstly we confirmed whether KIM-2 organoids regulate Stat3 and Stat5 phosphorylation in the same manner as the native gland, namely the downregulation or steady up-regulation of pStat5 and pStat3 respectively by removing PRL from the culture media (H/WD)[27]. Considering the close association of fatty and epithelial tissues in our model, we explored whether Stat

signalling profiles were altered in the presence of adipose, using the 3T3-L1 pre-adipocyte cell model in 2D trans-well cultures. The re-emergence of adipocytes is a feature of involuting tissue while lipid promotes IL-6/TNF mediated activation of Stat3 in hepatocytes[28] and its utilization by the epithelium has been shown to sensitize these cells to programmed cell death mechanisms[29].

In a similar manner to results previously demonstrated over shorter timescales[30], our study clearly showed a steady accumulation of pStat3 under H/WD conditions over a 4 day time period, elevated from an initial baseline following 2 weeks lactogenic treatment (Involution day0) (Fig S1a). Stat3 is constitutively expressed, although not phosphorylated, in all culture conditions as observed in vivo. Additionally pStat3 activity was accompanied by increases in the active forms of the lysosomal enzymes cathepsins L and B as well as the lipidated form of LC3B, LC3B-II indicative of ongoing autophagy. In the trans-well co-culture model, KIM-2 cells demonstrated a similar up-regulation of pStat3 regardless of 3T3-L1 differentiation status (Fig S1b). However, immunoblotting of cleaved caspase 3 (cc3) clearly showed a peak accumulation at 48hrs following H/WD, and this up-regulation was attenuated by the presence of adipose in a trans-well model. It is also interesting to note the loss of phosphorylated Akt during H/WD, a common survival pathway in many cell systems. Thus, important aspects of involution can be mimicked in our 3D culture model.

Prolactin withdrawal results in KIM-2 organoid regression and Stat3-mediated cell death in the 3D model.

An involution phenotype was induced by H/WD for a total of 96hrs duration in 3D 3T3-L1/KIM-2 co-cultures. Additionally, a positive control for Stat3 mediated cell death, which occurs during involution, was provided by OSM treatment (25ng/mL) which activates Stat3 in mammary epithelial cells *in vitro* and *in vivo* [30,9]. OSM was applied for the duration of the 96hr experimental involution period with media replenishment every 24hrs. Under conditions of H/WD, organoids underwent morphological changes becoming elongated and more discontinuous in nature (Fig 2a, d). Systematic image analysis (Fig 2b, c) demonstrated a reduction in total lumen area and lumen frequency accompanied by an increase in organoid aspect ratio (Fig 2d).

Immunohistochemical analysis revealed clear cell shedding into lumina in a similar manner to the gland *in vivo* (Fig 3a) although a proportion of cells also shed into the stromal space. The presence of shed cells within a patent lumen was confirmed by dual staining of AQP-5 and MFGE8. MFGE8 (Milk fat globule-EGF-factor 8/lactadherin) is a milk glycoprotein which

has a critical role in mammary gland re-modelling during involution as it facilitates clearance of apoptotic cells[31]. In a similar manner cleaved caspase 3 (cc3) positive cells were observed within lumina, but also in the wall of epithelial structures as well as in the stromal space. The presence of cc3+ cells in the stromal space may reflect cell anoikis during scaffold seeding, or organoid formation failure in a subpopulation of structures resulting in partial polarity and basement membrane coverage at the basal margin.

The withdrawal or prolactin for a total of 96hr resulted in a progressive increase in phosphorylated Stat3 in the 3D coculture model, in a similar manner to 2D mono and co-cultures (Fig 3b). This was accompanied by a loss in β-casein expression that was more rapid under conditions of forced activation of Stat3 by OSM treatment. Prolactin withdrawal also resulted in increased pro and active forms of Cathepsin L by 96hrs, in addition to cc3. Despite the clear induction of cell death mediators, it is interesting to note that there was no associated loss in E-cadherin, possibly indicating the retention of ductal-type epithelial tissue with elongated morphologies.

MMPs have an important role in mammary gland development and involution [32,33]. An analysis of gene expression in a range of MMPs (Fig S2) demonstrated that both MMP3 and MMP9 were up-regulated following 96hr H/WD compared to mRNA abundance at 12days lactogenic differentiation. Additionally the expression of both of these genes was dependant upon co-culture status, with MMP-3 more strongly expressed in the absence of 3T3-L1 cells and a reciprocal expression profile for MMP-9. The regulation of MMPs during mammary involution has been demonstrated in previous studies [30] where large increases in gene expression for MMP-2,3 and 9 have been evident by 72 hrs involution [33].

We investigated cell death indicators further by scoring E-cadherin positive (ECAD+) cells for the apoptotic marker cc3, or p62 (sequestosome-1), an important molecule involved in recognising polyubiquitinated, aggregated and misfolded cargo proteins for incorporation into autophagic vesicles for trafficking to the lysosome and clearance in autophagolysosomes[34]. The 96hr involution timecourse did not result in any significant fluctuation in the number of cc3+ apoptotic cells per ECAD+ organoid, although an increasing trend was evident over the 96hr period that was independent of OSM treatment (Fig 3c). In order to assess whether apoptosis could be induced in this model, we withdrew serum in the presence of lactogenic hormones and observed an over 2-fold increase in the number of cc3 positive cells (Fig S3).

In contrast, an analysis of autophagic flux revealed an increased cytoplasmic level of p62+ puncta in ECAD+ cells under H/WD at both 24hr and 96hrs ($p<0.05$) (Fig 3d). This was further increased by the application of OSM, implicating Stat3 signalling in either modulating the rate of autophagic flux or in the resolution of autophagy. It is interesting to note the transient increase in p62+ expression at 24hrs followed by a pronounced decay, with levels returning to baseline values by 96hrs. This is against a background of an increasing lysosomal compartment, as measured by western blot for LAMP-2 (Fig3b). These data could indicate biochemical adaptation to an initial stimulus of H/WD +/- OSM treatment, particularly considering the observed increase (H/WD) or amplification (H/WD + OSM) in pStat3 signal.

We explored these responses further by disrupting autophagosome and lysosome fusion[35] by treating 24hr H/WD +/- OSM samples with the V_0ATPase inhibitor Bafilomycin A_1 (Baf). Optimal Bafilomycin concentration was determined previously by staining KIM-2 cells with LysoTracker ® Red dye and noting the minimal concentration required to inhibit acidification of the lysosomal compartment (50nM) (Fig S4). Bafilomycinin treatment for 5hrs resulted in a notable increase in the frequency of p62 puncta, an effect that was amplified in the presence of OSM (Fig 3e). Since OSM treatment resulted in a partial increase in the number of p62+ puncta compared to bafilomycin treatment, and the combined action of both mediators was synergistic, we can deduce that it is more likely that Stat3 activation increases cellular autophagic flux rather than blocking the resolution of autophagy.

The inflammatory phenotype of KIM-2 cells is modulated in the presence of macrophages when cultures under involution conditions.

Considering the influence of macrophages on glandular development coupled to their characteristic influx in the later stages of involution, it is reasonable to propose that their presence influences mammary epithelial phenotype. The porous nature of our 3D *in vitro* system is applicable to studies of this type, whereby differing cell types can be introduced to established cultures in 3D.

The monocyte/macrophage cell line RAW-264.7 was seeded at 10^5 cells/mL within a subset of 3D KIM2/3T3-L1 cultures, 24hrs prior to the withdrawal of PRL (Fig 4a). This seeding density is comparable to macrophage abundance within the mammary gland, although levels are variable throughout the estrous cycle[36]. Macrophages seeded within this *in vitro* system became closely associated with epithelial organoids, visualized by confocal live-cell imaging (Fig 4b). This close association of macrophages with alveoli of the lactating gland has been

previously described, and is dependent on the expression of CSF-1[15]. The addition of a stromal component to our model system is advantageous in this respect, since expression of CSF-1 and to a lesser extent monocyte chemotactic protein-1 (MCP-1) are transiently up-regulated over a 12 day 3T3-L1 adipogenic time course (Fig S5a). Re-emmergence of adipose tissue is an important feature of involution and it is possible that this pattern of expression coincides with the infiltration of macrophages into the gland from 3 days *in vivo*. In addition, PPARγ, a critical adipogenesis regulator is a potent M2 inducible factor[37].

We performed an immunohistochemical analysis of the M2/anti-inflammatory marker arginase-1 (ARG1) on sections of our involution model (Fig 4c). ARG1/ECAD double positive cells increased in frequency with the withdrawal of PRL, indicating that KIM-2 switch their phenotype from differentiated milk-producing cells to express a marker of the M2 anti-inflammatory monocyte/macrophage lineage. Infiltrating macrophages undergo conversion to the M2 phenotype within involuting gland *in vivo* [19] and we confirmed the ability of RAW-264.7 cells to M2 conversion prior to co-culture analysis, exploring expression of ARG1 and YM-1 coupled to the down-regulation of the M1 marker iNOS under 10ng/mL IL-4 for 24hrs (Fig S5b). In an earlier study IL-4 cytokine expression was shown to be up-regulated by lactogenic KIM2 cells[38]. Interestingly, in the presence of RAW cells, the M2 phenotypic switch in KIM2 cells is negated from 48hrs H/WD onwards ($p<0.05$) (Fig4,d). There is now a consensus that luminal mammary epithelial cells increase their expression of phagocytic markers including CD14[39] [40,19] to allow for the uptake of shed cells and milk during involution prior to the influx of professional phagocytes.

Conclusions.

This paper describes a complex *in vitro* model of mammary gland generated *de novo* through the combination of essential tissue cell types within 3D engineered scaffolds of natural biomaterials. Within the model, organotypic mammary tissues develop and die in a physiological manner under the control of lactogenic hormones, demonstrating that such models are suitable *in vitro* platforms for the study of cancer development in which these processes are disrupted. Certain limitation of the current model should be highlighted, however. Firstly milk stasis through absence of suckling is the initial trigger for LIF induced phosphorylation of Stat3 and subsequent involution [41]. Three-dimensional models of the type presented are static environments where milk is synthesized into a closed system, thereby potentially triggering pro-involution conditions spontaneously. Secondly, physiological involution within our system can only take place within polar mammary organoids, the

frequency of which is limited to approximately 70% in 7.5%HA/col scaffolds [1]. This residual tissue component may complicate signalling microenvironments and data analyses.

Many 3D *in vitro* models of mammary tissue have been described, however this is the first to our knowledge that aims to reflect complex tissue remodelling processes that occur in the involuting gland following pregnancy and lactation. The model was used to highlight the role of Stat3 signalling in epithelial autophagic processes during the first 96hrs following H/WD, mimicked in our mammary involution model. Furthermore, this model demonstrates that macrophages present in the latter stages of involution can regulate mammary epithelial phenotype, reflecting the power of such models to study cell interactions in defined *in vitro* microenvironments. Models of this type form simple laboratory tools that are amenable to scale-up. Furthermore the murine cell lines of the current model could be readily replaced by human cell lines, primary cells or tissue biopsy specimens, forming powerful diagnostic platforms or predictors of therapeutic drug response.

Figure captions.

Fig 1 3D *in vitro* culture supports physiological mammary organoid formation. a) KIM2 cells were cultured for up to 4 days on 2D plastic or collagen type 1 prepared as thin film surfaces or porous freeze dried 3D scaffolds. 3D culture enables expression of glycosylated AQP5. b) Schematic of 3D involution model preparation. c) In co-culture with differentiated 3T3-L1, KIM2 cells form numerous branched interconnecting ductal and epithelial structures (confocal z-stack. bar = 50μm). In transverse section these display polar AQP5 towards the luminal cell surface (c, inset bar= 25μm) together with apical tight junctions (ZO1) surrounded by basement membrane (Laminin). In the co-culture model Ecad+ organoids are surrounded by fatty (Perilipin+) stromal tissue (bars = 50μm.

Fig 2. Morphological analysis of in vitro involution model. a) Hormone withdrawl triggered involution results in collapse of lumen structure and disaggregation of organoids (bar = 50μm). b) Image analysis of organoids was conducted using image j software, manually recording the boundary of organoids with associated lumens (L). d) Organoid morphologies described by lumen area, lumen frequency and aspect ratio (AR). AR is a function of long axis (l) to short axis ratios calculated from a software applied best-fitting ellipse (imagej).

Fig 3. 3D model recapitulates *in vivo* involution phenotype and Stat3 mediated cell death mechanisms. a) Immunohistochemical evaluation of KIM-2 mammary organoids during H/WD showing MFGE8+ cell shedding into an organoid lumen at 48hrs H/WD. Cleaved caspase-3 cells are visible within organoid luminal cavities and epithelial organoid walls throughout H/WD as well as p62+ cytoplasmic puncta (bars = 50μm). b) Western analysis of involution samples +/- application of OSM. c,d) quantification of cc3 and p62 immunohistochemical data, proportional to expression in control samples (no PRL withdrawal), reveals Stat3 dependent expression of p62 (*= $p<0.05$, **= $p<0.01$, #= $p<0.05$, n=5). e) Analysis of autophagic mechanism by application of bafilomycin results in increased p62+ puncta frequency in a Stat dependent manner n=3.

Fig 4 Macrophage influx model of involution modulates the phenotype of KIM-2 cells. a) Schematic of macrophage addition prior to the initiation of involution by H/WD. b) live-cell confocal imaging of cell-tracker (red) labelled macrophages associated with GFP labelled KIM2 organoids at 24hrs 3D co-culture. Arginase-1 expression in ecad+ KIM2 cells (c) is attenuated by the addition of RAW macrophages (d). Bars = 50μm

Supplemental Fig1. KIM-2 cells recapitulate activation of pStat3 in both 2D monoculture (a) and 2D trans-well co-culture (b) conditions. Adipose was not found to have an effect on the level of pStat3 signalling in the model, although cleaved caspase 3 is more prevalent in the absence of differentiated 3T3-L1.

Supplemental Fig 2. Analysis of MMP gene expression during H/WD in 3D coculture model.

Supplemental Fig 3. Immunohistochemical cc3 quantification in Ecad positive cells at the 48hr involution timepoint under conditions of H/WD, +/-OSM and pan-caspase OPH inhibitor Q-VD (20μM). Additionally caspase was quantified under conditions of serum withdrawal in the presence of lactogenic Prl stimulation. $n>3$ for all samples.

Supplemental Fig 4. KIM2 cells loaded with Lysotracker ® Red to monitor acidic lysosome compartment with increasing Bafilomycin concentration.

Supplemental Fig 5. a) CSF-1 and MCP-1 are regulated in 3T3-L1 with adipogenic conversion. b) RAW 264.7 cells undergo M2 conversion with IL-4 treatment.

Experimental.

Collagen/hyaluronic acid scaffold and film fabrication

3D collagen and collagen/HA (7.5 wt%) scaffolds with controlled porosity were fabricated using a freeze drying technique with subsequent cross-linking in aqueous 1-Ethyl-3-[3-dimethylaminopropyl]carbodiimide hydrochloride (EDC) in the presence of *N*-hydroxysuccinimide (NHS) as detailed earlier[24]. Resultant scaffolds were carefully cut into discs of 10mm diameter with a 1mm maximum thickness to support nutrient delivery and 3D cell seeding. Films of pure collagen were prepared on 60mm tissue culture dishes (Nunc) as described previously [1] at the same time as 3D scaffolds and cross-linked in the same manner with EDC/NHS before being air-dried. Scaffolds and films were bathed in a 10x solution of gentamycin (2.5mg/mL) in phosphate buffered saline (PBS) for 24hrs followed by rinsing (x3) in PBS, prior to introduction of cells.

Cell culture and *in vitro* model preparation.

3T3-L1 cells (ATCC, Manassas, VA, USA) and KIM-2 cells [42] were maintained as described previously. RAW 267.4 cells (a kind gift from Dr. H. Laman, Department of Pathology, Cambridge, UK.) were maintained in DMEM (Gibco, Life Technologies, Paisley, UK) + 10% FCS (PAA, Som, UK). For a comparison of protein expression in 2D and 3D substrates, KIM2 cells were seeded at $3x10^5$ cells/cm^2 on plastic or monolayer films and in 3D scaffolds at $1x10^6$ cells/mL as described below. For 2D co-cultures, 3T3-L1 were plated at $3x10^4$/cm^2 in 6 well plates and maintained to confluence prior to terminal differentiation with lμM dexamethasone (DEX), 0.5 mM 3-iso-butyl-1-methylxanthine (IBMX) and 0.8mM insulin (ins) (48hrs) (all Sigma, Poole, UK), and subsequently maintained in DMEM+10%FCS + ins for a further week. KIM-2 cells were maintained at confluence on 6 well transwell inserts (0.4 μm^2 pores, Corning, NY, USA) under lacogenic culture conditions (DMEM:F12 + 10% FCS, 0.8mM ins, 0.2mM PRL, 1mM DEX and 17mM linoleic acid) for 2weeks, prior to co-culture with 3T3-L1 under involution conditions. Involution was triggered by removal of PRL from lactogenic culture media with and without OSM supplementation (25ng/mL). 3D scaffolds were prepared for primary cell seeding by eliminating rinse solution with centrifugation (500*g*) on cell strainers. Compressed scaffolds were then swelled by immersing in $1x10^6$ cells/mL of either 3T3-L1 or KIM-2 cell suspensions to achieve homogenous 3D seeding. For 3D co-cultures, pre-seeded scaffolds were carefully blotted prior to the drop-wise addition of KIM-2 cells ($1x10^6$ cells/mL) or RAW 267.4 ($1x10^5$ cells/mL). For 3D involution conditions, adipogenesis was initiated as described above for 2weeks, prior to the introduction of KIM-2 cells. Following 48hrs KIM-2/3T3L1 equilibration, KIM-2 cells were differentiated with lactogenic media for 12 days. Involution was induced as described above for a total of 96hrs

+/- OSM addition. In macrophage influx studies RAW cells were added to 3D cultures 24hrs prior to H/WD. Involution control samples (receiving PRL continuously) were taken at both 0hrs and 96hrs.

Live cell imaging.

KIM-2 cells transfected with an MSCV-IRES-GFP empty vector (a kind gift from Prof. Göttgens, Department of Haematology, Cambridge, UK), were seeded into scaffolds at $1x10^6$ cell /mL and co-cultured with adipogenic 3T3-L1 in 3D scaffolds as described above. RAW 267.4 macrophages were loaded with 10 mM cell tracker dye (Celltracker red ® CMTPX, Life Technologies) in whole media for 30 minutes prior to seeding in 3D co-culture at $1x10^5$ cells/mL. Scaffolds were removed to an environment chamber of a confocal microscope (Leica TCS SP II, Leica Biosystems, Germany) and analyzed by laser excitation of GFP and cell tracker dye at 488 nm and 543 nm respectively using proprietary software (Leica Biosystems)

Immunodetection

Immunohistochemistry was carried out on paraffin-embedded sections as described previously[1]. Antibodies (all Cell Signalling Technology, USA, unless otherwise stated) were prepared to the following dilutions in 10% sera + PBS + 0.1%Tween20; Ecad (610182, BD Biosciences, Oxon, UK, 1/500), ZO-1 (MAB 1570, Millipore, USA, 1/250), AQP5 (AB3559, Millipore, 1:200), Laminin (ab11575, Abcam, Cambs, UK, 1:200), Cleaved-caspase 3 (CC3, 9661S, 1:200). MFGE8 (a kind gift from Prof Nagata, Kyoto University, Japan, 1:200), ARG-1 (AB91279, Abcam, 1:250), p62 (SQSTM1 MQL, 1:200), Perilipin (D1D8, 1:200). Signal was detected using Alexa-488, Cy-3 and Alexa-647 conjugated secondary antibodies (all Life Technologies) bisbenzimide-Hoechst 33342 nuclear staining and fluorescence microscopy with data capture (Zeiss AxioCam/Axioplan 3, Zeiss, Germany). Immunoblotting and signal detection was carried out as previously described (Khaled, 2007) with protein loading adjusted by densitometric lane analysis (Quantity One, Biorad, CA, USA) of β-actin (Ab8227-50, Abcam) or tubulin (ab6160, Abcam). Antibodies were prepared at the following dilutions is tris-buffered saline + 0.1% Tween20; total Stat3 (9132) 1:1000, P-Stat3 (9131) 1:1000, P-Akt (9271) 1/1000), LC3B (2775) 1:1000, Cathepsin L (MAB9521, R&D systems, MN, USA) 1:1000, Cathepsin B (ab33538, Abcam. 1:1000), AQP-5 (1:1000), β-casein (a gift from Bert Binas, 1:10000), Ecad (1/2500). Signal was detected using HRP-conjugated secondary antibodies (Dako), and ECL, ECL prime (GE healthcare) or Millipore detection reagents using manufacturers protocols.

Image analysis and statistics

Whole organoid and associated lumen morphologies were traced using the freehand selection tool in image j software (fig2b). Organoid aspect ratios were calculated by image j, dividing long axis (l) and short axis (s) of best fitting ellipse (fig2 c) applied to organoid circumferences. All statistical analyses by *a priori* ANOVA and student T Test were performed using Excel data analysis toolpak (Microsoft, CA, USA).

Gene expression analysis.

Gene expression by PCR was carried out using standard procedures as previously described. Validated sequences for the following genes were obtained from Primerbank[43] *ARG-1* (7106255a), *YM-1,* (6753416a1), *inos-2* (6754872a1), *PPARγ* (6755138a1), *CSF-1* (192801a1), *MCP-1* (6755430a1), *MMP-11* (6678894a1) and *MMP-14* (31982191a1). Sequences for Cyclophilin, MMP 2,3 and 9 were validated and published previously [19]. All primers were obtained from Sigma-Aldrich.

References.

1. J. J. Campbell, N. Davidenko, M. M. Caffarel, R. E. Cameron, and C. J. Watson, *PLoS ONE*, 2011, **6**, e25661.
2. R. Clarkson, M. Boland, E. Kritikou, J. Lee, T. Freeman, P. Tiffen, and C. Watson, *Mol Endocrinol*, 2006, **20**, 675–685.
3. S. Pensa, C. J. Watson, and V. Poli, *J Mammary Gland Biol*, 2009, **14**, 121–129.
4. J. Bollrath and F. R. Greten, *EMBO Rep*, 2009, **10**, 1314–1319.
5. J. O'Brien, T. Lyons, J. Monks, M. S. Lucia, R. S. Wilson, L. Hines, Y.-G. Man, V. Borges, and P. Schedin, *American Journal of Pathology*, 2010, **176**, 1241–1255.
6. T. R. Lyons, J. O'Brien, V. F. Borges, M. W. Conklin, P. J. Keely, K. W. Eliceiri, A. Marusyk, A.-C. Tan, and P. Schedin, *Nat. Med.*, 2011, **17**, 1109–1115.
7. L. R. Lund, J. Rømer, N. Thomasset, H. Solberg, C. Pyke, M. J. Bissell, K. Danø, and Z. Werb, *Development*, 1996, **122**, 181–193.
8. R. S. Chapman, P. C. Lourenco, E. Tonner, D. J. Flint, S. Selbert, K. Takeda, S. Akira, A. R. Clarke, and C. J. Watson, *Genes Dev*, 1999, **13**, 2604–2616.
9. P. A. Kreuzaler, A. D. Staniszewska, W. Li, N. Omidvar, B. Kedjouar, J. Turkson, V. Poli, R. A. Flavell, R. W. E. Clarkson, and C. J. Watson, *Nat. Cell Biol.*, 2011, **13**, 303–309.
10. S. Shen, M. Niso-Santano, S. Adjemian, T. Takehara, S. A. Malik, H. Minoux, S. Souquere, G. Mariño, S. Lachkar, L. Senovilla, L. Galluzzi, O. Kepp, G. Pierron, M. C. Maiuri, H. Hikita, R. Kroemer, and G. Kroemer, *Molecular Cell*, 2012, **48**, 667–680.
11. I. Teplova, F. Lozy, S. Price, S. Singh, N. Barnard, R. D. Cardiff, R. B. Birge, and V. Karantza, *Autophagy*, 2013, **9**, 459–475.
12. R. Mathew, C. M. Karp, B. Beaudoin, N. Vuong, G. Chen, H.-Y. Chen, K. Bray, A. Reddy, G. Bhanot, C. Gelinas, R. S. DiPaola, V. Karantza-Wadsworth, and E. White, *Cell*, 2009, **137**, 1062–1075.
13. A. Van Nguyen and J. W. Pollard, *Developmental Biology*, 2002, **247**, 11–25.
14. J. O'Brien, H. Martinson, C. Durand-Rougely, and P. Schedin, *Development*, 2012, **139**, 269–275.
15. V. Gouon-Evans, E. Y. Lin, and J. W. Pollard, *Breast Cancer Res*, 2002, **4**, 155–164.
16. D. E. Gyorki, M.-L. Asselin-Labat, N. Van Rooijen, G. J. Lindeman, and J. E. Visvader, *Breast Cancer Res*, 2009, **11**, R62.
17. V. Dayan, G. Yannarelli, F. Billia, P. Filomeno, X.-H. Wang, J. E. Davies, and A. Keating, *Basic Res Cardiol*, 2011, **106**, 1299–1310.
18. V. E. Miron, A. Boyd, J.-W. Zhao, T. J. Yuen, J. M. Ruckh, J. L. Shadrach, P. van Wijngaarden, A. J. Wagers, A. Williams, R. J. M. Franklin, and C. ffrench-Constant, *Nat Neurosci*, 2013, **16**, 1211–1218.
19. K. Hughes, J. A. Wickenden, J. E. Allen, and C. J. Watson, *J. Pathol.*, 2012, **227**, 106–117.
20. M. Skowron-zwarg, S. Boland, N. Caruso, C. Coraux, F. Marano, and F. Tournier, *Experimental Cell Research*, 2007, **313**, 2695–2702.
21. Y. Garfias, A. Navas, H. J. Pérez-Cano, J. Quevedo, L. Villalvazo, and J. C. Zenteno, *Mol. Vis.*, 2008, **14**, 756–761.

22. T. Matsuzaki, N. Machida, Y. Tajika, A. Ablimit, T. Suzuki, T. Aoki, H. Hagiwara, and K. Takata, *Histochem Cell Biol*, 2005, **123**, 501–512.
23. G. Hendriks, *J Biol Chem*, 2003, **279**, 2975–2983.
24. N. Davidenko, J. J. Campbell, E. S. Thian, C. J. Watson, and R. E. Cameron, *Acta Biomaterialia*, 2010, **6**, 3957–3968.
25. J. M. Shillingford, K. Miyoshi, G. W. Robinson, B. Bierie, Y. Cao, M. Karin, and L. Hennighausen, *J. Histochem. Cytochem.*, 2003, **51**, 555–565.
26. A. Mobasheri, B. H. Kendall, J. E. J. Maxwell, A. V. Sawran, A. J. German, D. Marples, M. R. Luck, and M. D. Royal, *Acta histochemica*, 2011, **113**, 137–149.
27. C. J. Watson, *J Mammary Gland Biol*, 2001, **6**, 115–127.
28. E. J. Park, J. H. Lee, G.-Y. Yu, G. He, S. R. Ali, R. G. Holzer, C. H. Osterreicher, H. Takahashi, and M. Karin, *Cell*, 2010, **140**, 197–208.
29. C. Gajate, F. Gonzalez-Camacho, and F. Mollinedo, *Biochemical and Biophysical Research Communications*, 2009, **380**, 780–784.
30. P. G. Tiffen, N. Omidvar, N. Marquez-Almuina, D. Croston, C. J. Watson, and R. W. E. Clarkson, *Mol Endocrinol*, 2008, **22**, 2677–2688.
31. K. Atabai, R. Fernandez, X. Huang, I. Ueki, A. Kline, Y. Li, S. Sadatmansoori, C. Smith-Steinhart, W. Zhu, R. Pytela, Z. Werb, and D. Sheppard, *Mol Biol Cell*, 2005, **16**, 5528–5537.
32. P. P. Lee, J. J. Hwang, L. Mead, and M. M. Ip, *J. Cell. Physiol.*, 2001, **188**, 75–88.
33. R. Zaragoza, A. Gimeno, V. J. Miralles, E. R. Garcia-Trevijano, R. Carmena, C. Garcia, M. Mata, I. R. Puertes, L. Torres, and J. R. Vina, *AJP: Endocrinology and Metabolism*, 2006, **292**, E1140–E1148.
34. J. Moscat and M. T. Diaz-Meco, *Cell*, 2009, **137**, 1001–1004.
35. A. Yamamoto, Y. Tagawa, T. Yoshimori, Y. Moriyama, R. Masaki, and Y. Tashiro, *Cell Struct. Funct.*, 1998, **23**, 33–42.
36. A. C. L. Chua, L. J. Hodson, L. M. Moldenhauer, S. A. Robertson, and W. V. Ingman, *Development*, 2010, **137**, 4229–4238.
37. R. Stienstra, C. Duval, S. Keshtkar, J. van der Laak, S. Kersten, and M. Müller, *J Biol Chem*, 2008, **283**, 22620–22627.
38. W. T. Khaled, E. K. C. Read, S. E. Nicholson, F. O. Baxter, A. J. Brennan, P. J. Came, N. Sprigg, A. N. J. McKenzie, and C. J. Watson, *Development*, 2007, **134**, 2739–2750.
39. V. A. Fadok, D. L. Bratton, S. C. Frasch, M. L. Warner, and P. M. Henson, *Cell Death Differ*, 1998, **5**, 551–562.
40. T. Stein, J. S. Morris, C. R. Davies, S. J. Weber-Hall, M.-A. Duffy, V. J. Heath, A. K. Bell, R. K. Ferrier, G. P. Sandilands, and B. A. Gusterson, *Breast Cancer Res*, 2004, **6**, R75–91.
41. C. J. Watson, *Breast Cancer Res*, 2006, **8**, 203.
42. K. E. Gordon, B. Binas, R. S. Chapman, K. M. Kurian, R. W. Clarkson, A. J. Clark, E. B. Lane, and C. J. Watson, *Breast Cancer Res*, 2000, **2**, 222–235.
43. X. Wang and B. Seed, *Nucleic Acids Res*, 2003, **31**, e154.

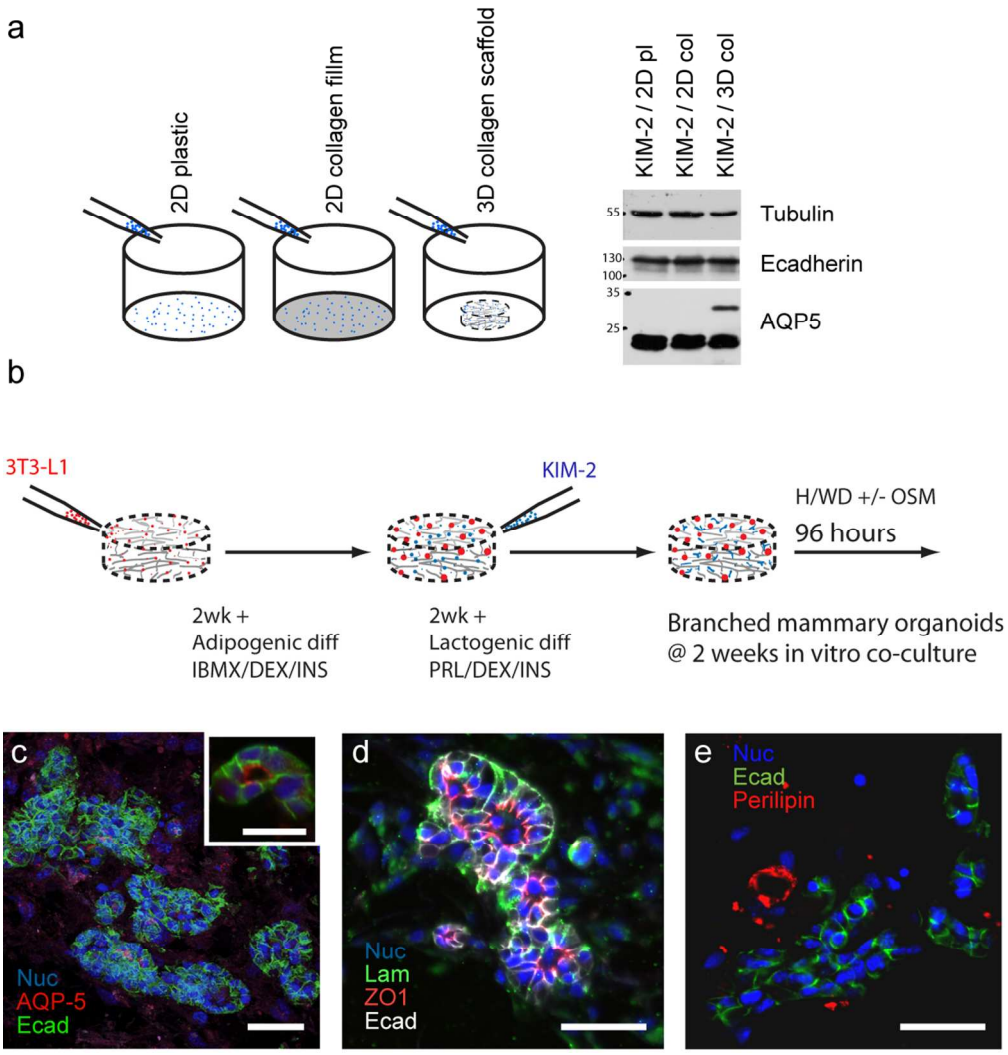

Figure 1. 3D in vitro culture supports physiological mammary organoid formation. a) KIM2 cells were cultured for up to 4 days on 2D plastic or collagen type 1 prepared as thin film surfaces or porous freeze dried 3D scaffolds. 3D culture enables expression of glycosylated AQP5. b) Schematic of 3D involution model preparation. c) In co-culture with differentiated 3T3-L1, KIM2 cells form numerous branched interconnecting ductal and epithelial structures (confocal z-stack. bar = 50μm). In transverse section these display polar AQP5 towards the luminal cell surface (c, inset bar= 25μm) together with apical tight junctions (ZO1) surrounded by basement membrane (Laminin). In the co-culture model Ecad+ organoids are surrounded by fatty (Perilipin+) stromal tissue (bars = 50μm.
108x112mm (300 x 300 DPI)

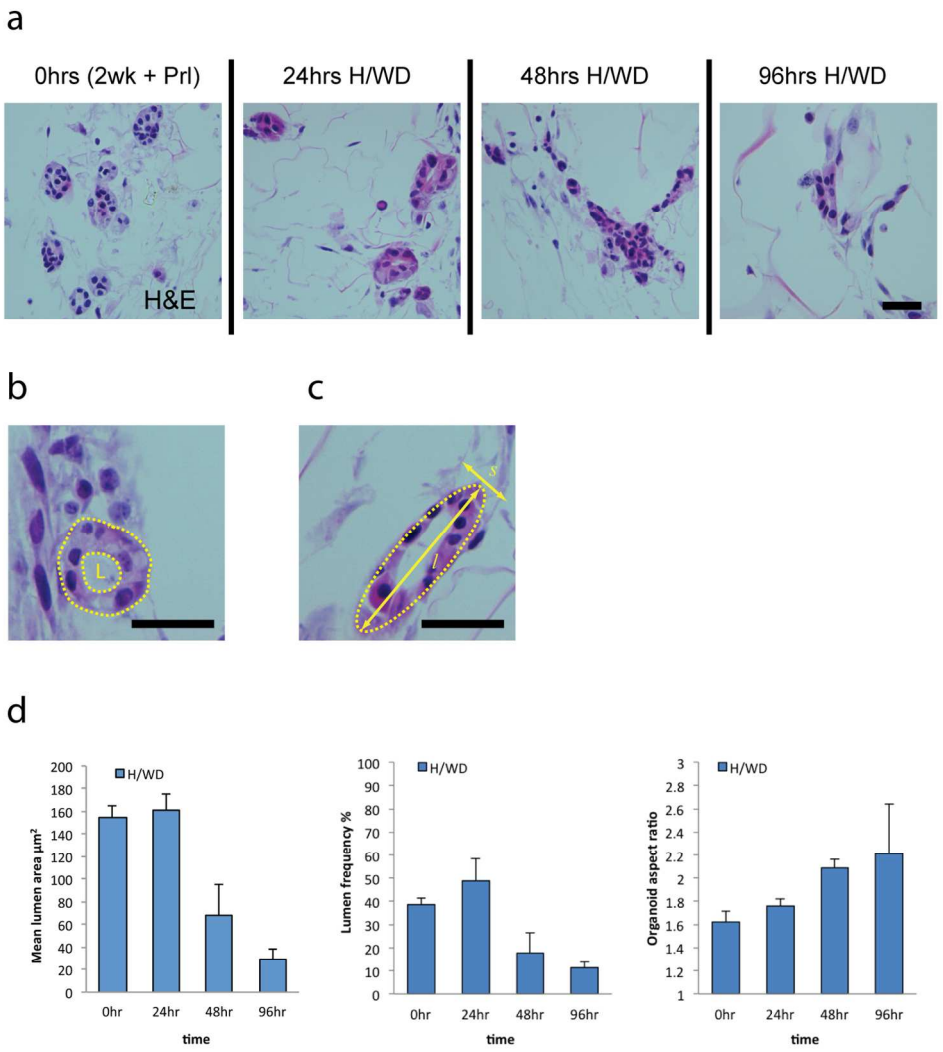

Figure 2. Morphological analysis of in vitro involution model. a) Hormone withdrawl triggered involution results in collapse of lumen structure and disaggregation of organoids (bar = 50µm). b) Image analysis of organoids was conducted using image j software, manually recording the boundary of organoids with associated lumens (L). d) Organoid morphologies described by lumen area, lumen frequency and aspect ratio (AR). AR is a function of long axis (l) to short axis ratios calculated from a software applied best-fitting ellipse (imagej).
131x140mm (300 x 300 DPI)

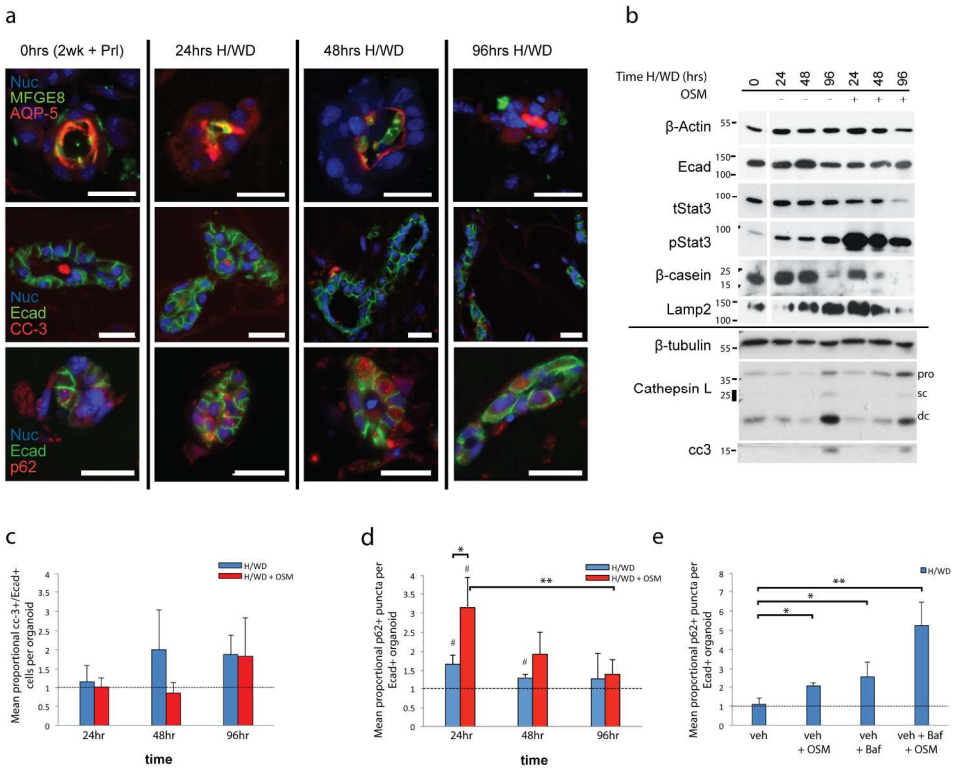

Fig 3. 3D model recapitulates in vivo involution phenotype and Stat3 mediated cell death mechanisms. a) Immunohistochemical evaluation of KIM-2 mammary organoids during H/WD showing MFGE8+ cell shedding into an organoid lumen at 48hrs H/WD. Cleaved caspase-3 cells are visible within organoid luminal cavities and epithelial organoid walls throughout H/WD as well as p62+ cytoplasmic puncta (bars = 50μm). b) Western analysis of involution samples +/- application of OSM. c,d) quantification of cc3 and p62 immunohistochemical data, proportional to expression in control samples (no PRL withdrawal), reveals Stat3 dependent expression of p62 (*= p<0.05, **= p<0.01, #= p <0.05, n=5). e) Analysis of autophagic mechanism by application of bafilomycin results in increased p62+ puncta frequency in a Stat dependent manner n=3.
210x182mm (300 x 300 DPI)

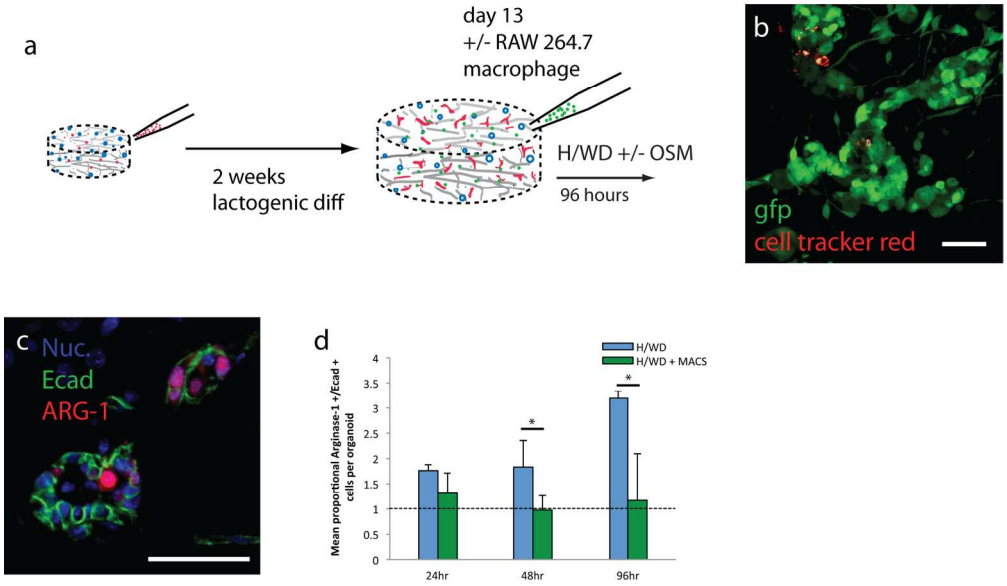

Figure 4. Macrophage influx model of involution modulates the phenotype of KIM-2 cells. a) Schematic of macrophage addition prior to the initiation of involution by H/WD. b) live-cell confocal imaging of cell-tracker (red) labelled macrophages associated with GFP labelled KIM2 organoids at 24hrs 3D co-culture. Arginase-1 expression in ecad+ KIM2 cells (c) is attenuated by the addition of RAW macrophages (d).Bars = 50μm.
159x96mm (300 x 300 DPI)

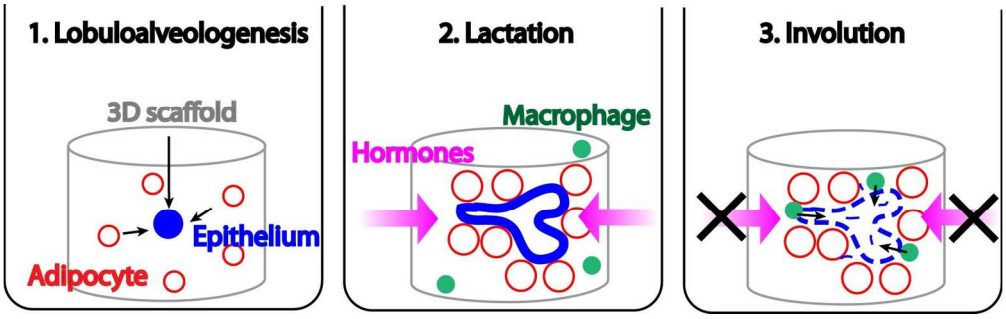

An in vitro model of mammary gland supporting 3D cell-cell and cell-matrix interactions demonstrates complete in vivo-like neo-tissue formation and remodelling processes (involution) under hormonal control.
150x46mm (300 x 300 DPI)